Theoretical Insights into Ultrafast-decaying and Long-lived States of ortho-Nitrophenol upon Photoexcitation in the Gas Phase

Satoi Wada,[†] Takuro Tsutsumi,[†] Kenichiro Saita,[†] Taro Sekikawa,[‡] and Tetsuya Taketsugu[*,†,¶]

†*Department of Chemistry, Faculty of Science, Hokkaido University, Sapporo, 060-0810, Japan*

‡*Department of Applied Physics, Faculty of Engineering, Hokkaido University, Sapporo, 060-8628, Japan*

¶*Institute for Chemical Reaction Design and Discovery (WPI-ICReDD), Hokkaido University, Sapporo 001-0021, Japan*

E-mail: take@sci.hokudai.ac.jp

Abstract

Nitrophenols in the atmosphere are chromophore pollutants that absorb sunlight. Among them, *ortho*-nitrophenol (*o*-NP) stands out due to its strong intramolecular hydrogen bond, which facilitates excited-state intramolecular proton transfer (ESIPT) and influences its photoisomerization and dissociation. Time-resolved experiments have captured both ultrafast-decaying and long-lived signals. Here, we employ non-adiabatic molecular dynamics simulations and the Reaction Space Projector method to elucidate the photoinduced reactions of *o*-NP. Our simulations show that photoexcited *o*-NP in the $S_1(\pi\pi^*)$ state undergoes ultrafast ESIPT, followed by rapid decay through one of two non-adiabatic pathways: ultrafast internal conversion to the S_0 state and inter-system crossing (ISC) to the triplet states. Furthermore, trajectories undergoing ISC remain trapped in triplet states, with reverse ISC to the singlet states rarely observed. These trajectories are clearly linked to the long-lived excited-state signal, providing more conclusive computational evidence for the origin.

Nitrophenols (NPs) are ubiquitous atmospheric pollutants found in the gas phase and organic aerosols, primarily originating from agricultural emissions, biomass burning, and wood, coal, and fossil fuel combustion.[1] NPs absorb sunlight in the UV-visible region and are photoreactive,[2,3] resulting in a potential source of photochemical hydroxyl radical generation,[4] which contributes to ozone formation and photochemical smog.[5] Among NPs, *ortho*-nitrophenol (*o*-NP) is particularly notable due to the strong intramolecular hydrogen bond between its adjacent hydroxyl and nitro groups, which facilitates excited-state intramolecular proton transfer (ESIPT). ESIPT is a fundamental process in photochemistry and photophysics, playing a pivotal role in applications such as fluorescent sensors[6,7] and light-emitting materials.[8,9] Beyond ESIPT, the photochemical behavior of *o*-NP encompasses additional intriguing processes that have increasingly attracted substantial research attention even in the last few years.[10–14] These processes not only deepen our understanding of *o*-NP's reactivity but also contribute to the broader study of atmospheric chemistry and photochemical dynamics.

Over the past decade, the ultrafast photoexcited reactions of *o*-NP in the gas phase have been extensively investigated through experimental and theoretical studies.[11,15–18] A time-resolved spectroscopy study by Ernst *et al.* captured two ultrafast processes occurring on different time scales[15] following photoexcitation to the A-band state of *o*-NP in the gas phase. This A-band state has been assigned to the $S_1(\pi\pi^*)$ state, characterized by partial charge transfer from the benzene ring to the nitro group, as corroborated by *ab initio* and time-dependent density functional theory (TD-DFT) studies.[15,18,19] Theoretical analysis of excited states and potential energy surfaces, based on the complete active space self-consistent field (CASSCF)[15] and multi-reference second-order perturbation theory (CASPT2),[18] have provided mechanistic insights into these ultrafast processes. These include ESIPT on the $S_1(\pi\pi^*)$ state and subsequent internal conversion (IC) to the S_0 state. Additionally, experimental observations of a long-lived state[15,20] have been attributed to intersystem crossing (ISC) to triplet states. ISC rates in light-atom molecules are typically small due to weak spin-orbit coupling (SOC). However, according to El-Sayed's rule,[21] ISC can efficiently occur between states with differing orbital characters, such as $\pi\pi^*$ and $n\pi^*$ transitions in singlet and triplet states. A prior study[18] examined SOC profiles during the twisting of the hydrated nitro group (HONO) following ESIPT. The SOC between the $S_1(\pi\pi^*)$ and $T_2(n\pi^*)$ states was found to remain nearly constant during HONO twisting, while the SOC between the $S_1(\pi\pi^*)$ and $T_1(\pi\pi^*)$ states increased throughout this process. Several groups have performed non-adiabatic molecular dynamics (NAMD) simulations for *o*-NP.[11,12,16] However, the mechanisms proposed in these studies conflict with experimental results.[15] Nunes *et al.*[11] reported ultrafast ESIPT followed by IC to the S_0 state, but without evidence of a long-lived excited state and explicitly rejected the possibility of ISC. Xu *et al.*[16] suggested a slower ESIPT process (> 10 ps) rather than an ultrafast one and did not provide insights into the long-lived excited state, even though ISC was observed in their simulations. Vandaele *et al.*[12] demonstrated ISC in the gas phase but relied on TD-DFT, which is insufficient to discuss IC to the ground state. Moreover, their simulation time was too

short to address the long-lived signal. To date, no existing study has provided a mechanistic explanation that comprehensively describes experimental observations of ultrafast-decaying and long-lived signals.[15]

In this Letter, we unveil the excited state dynamics of *o*-NP upon photoexcitation to the $\pi\pi^*$ state using NAMD simulations. Building on our ongoing research, which began with a prior study,[18] we identified that limitations in the electronic structure methods employed in earlier studies[11,12,16] significantly influenced the results of dynamics simulations, often leading to potential misinterpretations. For instance, the lack of dynamic correlation[16] or insufficient active space[11] hindered the accurate representation of ultrafast ESIPT and ISC processes. These factors are critical for properly describing the energy levels and nature of the $\pi\pi^*$ and $n\pi^*$ states, which are key to understanding ISC mechanisms based on El-Sayed's rule.[21] Furthermore, poor characterization of the conical intersection (CI) between the ground and first excited states in TD-DFT[12] complicated the qualitative analysis of relaxation and subsequent dynamics. A previous single-state CASPT2 study[18] addressed a correction of energy levels and the characterization of the $\pi\pi^*$ and $n\pi^*$ states, as well as the ESIPT process followed by the twisting of the hydrated nitro group (HONO). However, it did not discuss relaxation dynamics via a CI or the subsequent dynamics due to the computational expense of employing the multi-state CASPT2 method in NAMD simulations. To overcome these limitations, we carefully validated and employed the mixed-reference spin-flip TD-DFT (MRSF-TDDFT)[22] method in this study. This approach allowed us to perform on-the-fly molecular dynamics simulations with improved accuracy and efficiency. Additionally, IC and ISC processes were treated on equal footing using the surface hopping method with the Zhu-Nakamura theory-based global switching algorithm.[16,23] The NAMD trajectories were analyzed using the Reaction Space Projector (ReSPer) method,[24–26] which visualizes dynamic trajectories in a reduced-dimensional space automatically constructed using reference structures. This combined methodology provides a robust approach for exploring the complex excited state dynamics of *o*-NP.

Figure 1 illustrates the potential energy profiles (top), selected internal coordinates (middle), and representative structures (bottom) along a *meta*-IRC pathway[27] originating from the Franck-Condon structure, where the *meta*-IRC refers to a steepest descent pathway starting from non-TS structure, in the $S_1(\pi\pi^*)$ state of *o*-NP, calculated at the MRSF-TDDFT level. The S_1 excitation energy is 4.41 eV, which is slightly overestimated compared to advanced wavefunction theories;[18,19] however, the electronic nature of partial charge transfer from the benzene ring to the nitro group is accurately reproduced. The MRSF-TDDFT-calculated spectrum in Fig. S1 reasonably reproduces the three absorption bands observed experimentally.[15] The pathway following the Franck-Condon excitation involves two key processes: ESIPT and HONO twisting. ESIPT, characterized by changes in hydrogen-oxygen bond lengths (r_{O1H2} and r_{O3H2}) and O-O distance (r_{O1O3}), occurs over the reaction coordinate range of 0–1.3 amu$^{1/2}$ Å (structure **I** to **II**). This is followed by HONO twisting – a rotation around the C-N bond (defined by dihedral angles $d_{O3N5C6C7}$ and $d_{O4N5C6C8}$), accompanied by a modest energy decrease (structure **II** to **III**). Those results are consistent with the results by CASPT2 method (See Fig. S2). HONO twisting is suggested to be relatively slower than ESIPT, likely due to its small energy change and the orthogonal nature of in-plane ESIPT and out-of-plane HONO twisting motions. During ESIPT, the T_2 state intersects with the S_1 state, but ISC is unlikely due to the rapid traversal of the intersection. In contrast, during HONO twisting, the T_1 state crosses near the S_0/S_1 crossing region. Although the SOC between S_1 and T_1 increases along this process,[18] due to the small SOC, IC is likely to dominate over ISC.

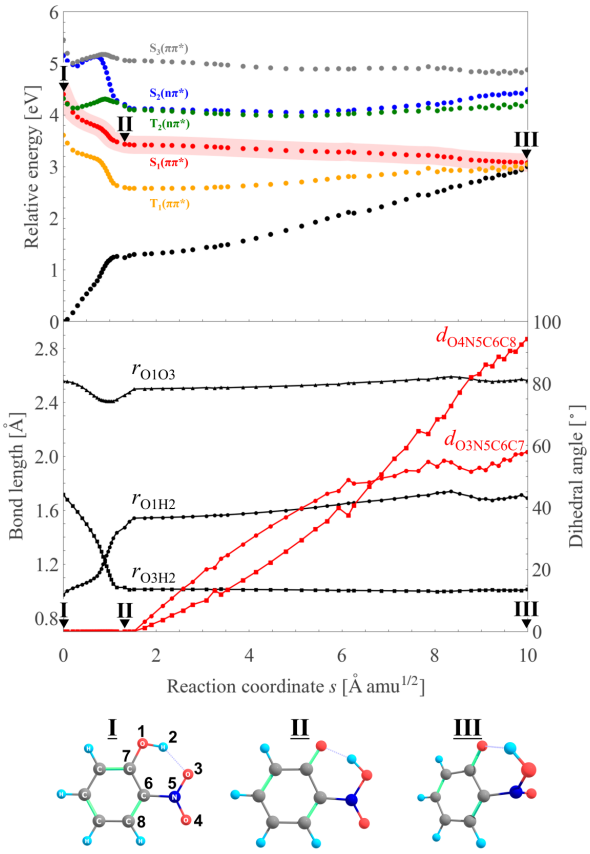

Figure 1: Profiles of potential energies (top) and internal coordinates (middle) along the *meta*-IRC pathway originating from the Franck-Condon structure in the S_1 state. Representative geometries are shown at the bottom: (**I**) at the FC point, (**II**) after the ESIPT, and (**III**) after the following HONO twist. Atom numbers are also shown in the structure (**I**).

Using the Zhu-Nakamura theory-based global switching algorithm,[23] NAMD simulations were performed to account for both IC and ISC processes. In these simulations, IC and ISC events were observed on the sub-picosecond timescale. **Figure 2** shows the time evolution of the population in each electronic state, while histograms of hopping times are provided in Fig. S4. The S_1 population gradually decreases before 200 fs, followed by exponential decay. This slow reduction in S_1 population results from IC between the S_1 and S_2 states, which occurred frequently before IC to the S_0 state, as shown in Fig. S4. Around 250 fs, the S_1 population begins to decrease rapidly, corresponding to the ultrafast-decaying signal within 200-300 fs.[15] Simultaneously, the S_0 and T_1 populations begin to increase, indicating that both IC and ISC processes contribute to the ultrafast-decaying signal observed experimentally.[15] ISC to

the triplet states occurs primarily between the S_1 and T_2 states. As shown in Fig. S4e, ISC between S_1 and T_1 states occurred 10 times, whereas ISC between S_1 and T_2 states occurred 60 times (Fig. S4f). By 2000 fs, most trajectories remain in either the S_0 or T_1 states. ISC between T_1 and S_0 states was rarely observed (see Fig S4d), indicating that the final population in the T_1 state corresponds to the long-lived excited state observed in previous experimental studies.[15,20]

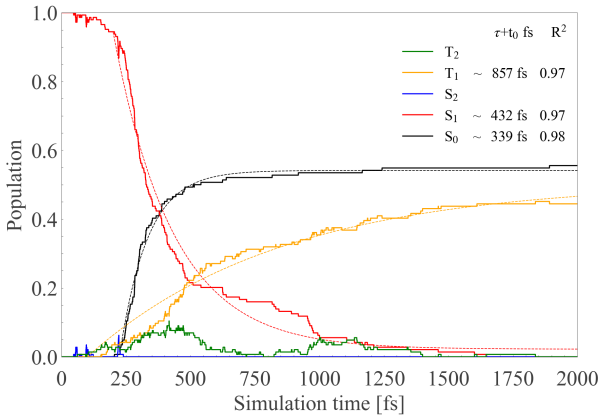

Figure 2: Time evolution of the populations in each electronic state obtained from NAMD simulations. The solid curves represent the actual data, while the dotted curves depict exponential fitting functions. The figure also includes calculated time constants ($\tau + t_0$) and the corresponding R^2 values, indicating the quality of the fit.

Each population of the S_1, S_0, and T_1 states was individually fitted to a single exponential function. The time constant for the decay of the S_1 was determined to be 432 fs, while the time constants for the appearance of the S_0 and T_1 states were 339 fs and 857 fs, respectively. The decay of the S_1 state are closely aligned with the single-exponential signal rise with a time constant of 433 $\pm$ 227 fs, as observed in the time-resolved experiment,[18] while the appearance of the S_0 or T_1 state is not. This is because the ionization energy range used to measure the signal is is deeper than the HOMO level (10.85 $\sim$ 11.30 eV).[18] Therefore, the observed signal are not directly associated with an ionization from an excited electron but are thought to reflect structural changes, particularly those involving the HONO group. Figure S5 shows time evolution of the dihedral angle along the trajectories, indicating that

the HONO group begins to twist out of the molecular plane in the initial 400 fs, which aligns well with the experimental time constant of 433 ± 227 fs. The dynamics of the HONO group continue after IC to the S_0 state (see Fig. 4c) and after ISC to the triplet states (see Fig. 4f) This interpretation could be further validated using time-resolved electron spin resonance spectroscopy, which can distinguish the spin-multiplicity of the molecule.

The ESTIP and HONO twisting processes in the dynamic trajectories were analyzed based on changes in geometries and electronic states over time. **Figure 3** illustrates the time evolution of the interatomic distance r_{O3H2} between the transferring hydrogen atom (H2) and the oxygen atom (O3) of the nitro group, and the interatomic distance r_{O1O3} between oxygen atoms of the hydroxyl and nitro groups during the first 200 fs following excitation, as well as the dihedral angles d_{O3N5C6C7} and d_{O4N5C6C8}, which represent the HONO twisting motion, over 500 fs in each trajectory (see Fig. 1 for atom numbering). The color of each line indicates the electronic state in which the trajectory resides. The light green line in Fig. 3a represents an exponential fitting function with a time constant of 13 fs, which is in good agreement with experimental observations (14 ± 6 fs).[15] After 100 fs, r_{O3H2} oscillates around 1 Å, confirming that ultrafast ESIPT in the S_1 ($\pi\pi^*$) state is rapidly completed along the dynamic trajectory, as predicted by the *meta*-IRC pathway. Subsequent IC and ISC dynamics are roughly classified based on the two dihedral angles, d_{O3N5C6C7} and d_{O4N5C6C8}. In Figs. 3(b) and 3(c), trajectories where both dihedral angles approach approximately 90° tend to undergo IC to the S_0 state, typically beginning after approximately 250 fs – significantly slower than the 14 ± 6 fs observed for ESIPT.[15] In contrast, trajectories with $d_{\mathrm{O3N5C6C7}} < 90°$ and $d_{\mathrm{O4N5C6C8}} < 60°$ tend to undergo ISC to the triplet states. Some trajectories undergo ISC to the triplet states before 250 fs, occurring faster than IC to the S_0 state.

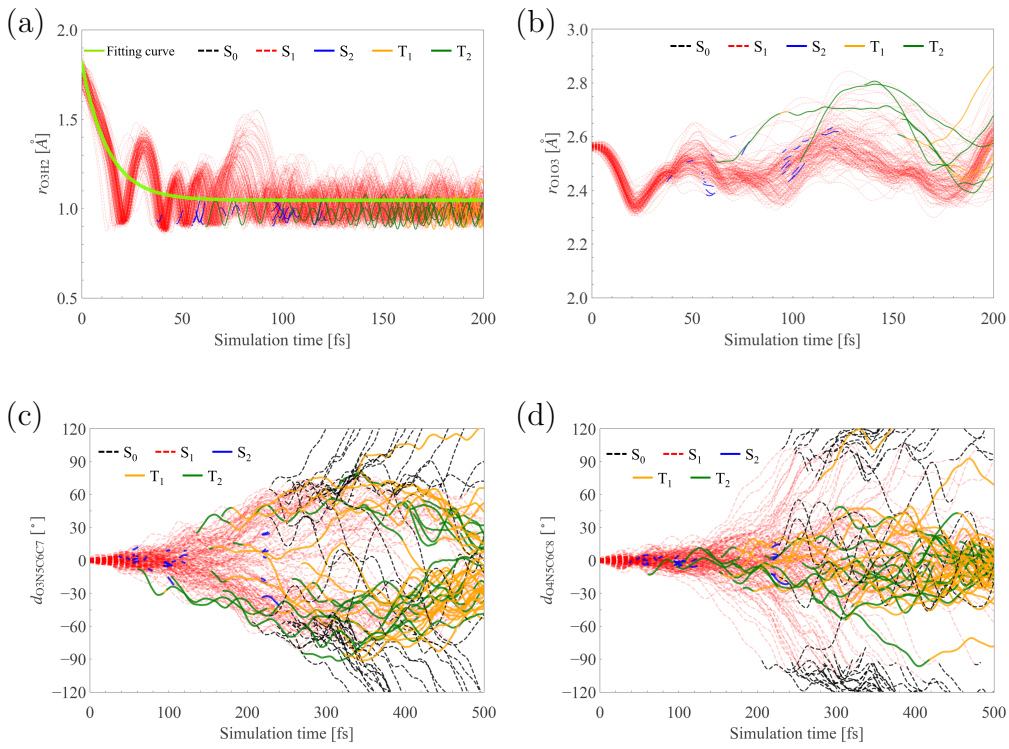

Figure 3: Time evolution of (a) the interatomic distance r_{O3H2} between the transferring hydrogen atom (H2) and the oxygen atom (O3) of the nitro group, along with a fitting curve for the averaged value during the first 200 fs, showing a time constant of 13 fs; (b) the interatomic distance r_{O1O3} between oxygen atoms of the hydroxyl (O1) and nitro (O3) groups; and the dihedral angles (c) d_{O3N5C6C7} and (d) d_{O4N5C6C8}, over 500 fs in each trajectory, as obtained from NAMD simulations. The color of each line indicates the electronic state in which the trajectory resides.

We analyze which minimum energy conical intersections (MECIs) and minimum energy seam of crossings (MESXs) are dynamically preferred. MECI and MESX structures were systematically explored using the GRRM program.[28,29] The full lists of MECI/MESX structures are provided in Figs. S6 and S7. Each hopping point was assigned to the nearest MECI/MESX structure based on the distance from the reference MECI/MESX structure. In our NAMD simulations, 350 transitions were observed following ESIPT. Figure S8 shows the dynamically accessed MECI/MESX structures and the number of transitions occurring near each MECI/MESX. The most frequent IC process between S_1 and S_0 occurred via MECI(S_0/S_1)1 (70 instances), as anticipated from the *meta*-IRC pathway. Interestingly,

IC between S_1 and S_2 occurred via MECI(S_1/S_2)1 (74 instances) near the FC structure, though many trajectories returned via the same MECI. ISC between S_1 and T_2 occurred via MESX(S_1/T_2)1, MESX(S_1/T_2)2, and MESX(S_1/T_2)4, with 23, 31, and 6 transitions, respectively. ISC was observed both when the molecule retained planar (MESX(S_1/T_2)1) and when it adopted twisted HONO configurations (MESX(S_1/T_2)2, MESX(S_1/T_2)4). Unlike IC, ISC disrupts the hydrogen bond, and hydrogen-bond-free MECIs were identified but were observed in fewer trajectories. The loss of hydrogen bonding at MESX(S_1/T_2)2 and MESX(S_1/T_2)4 suggests a preference for the ISC pathway in molecules without hydrogen bonds. ISC between S_1 and T_1 via MESX(S_1/T_1)1 occurred in only 10 transitions. Thus, the increasing T_1 population is primarily attributed to IC between T_1 and T_2 via MECI(T_1/T_2)3, which accounted for 124 transitions. Thus, IC between singlets or between triplets occurs mostly at a single MECI point, while ISC occurs at multiple MESX points, suggesting that the ISC process is inherently more complex than the IC process.

To further investigate ultrafast-decaying and long-lived dynamic trajectories beyond analysis based on intuitively-chosen internal coordinates, we constructed a two-dimensional reaction space using the Reaction Space Projector (ReSPer) method, which extracts principal coordinates (PCos) through a dimensionality reduction technique.[24–26] (See Computational Methods and Supporting Information for details.) We projected both the *meta*-IRC originating from the Franck-Condon point of S_0-EQ0 and the dynamic trajectories using the out-of-sample extension technique.[25] **Figure 4a** shows the two-dimensional reaction space generated by ReSPer, with cumulative contributions of 0.87% for the first two PCos. These two principal coordinates, PCo1 and PCo2, span the reduced-dimensional subspace and correspond primarily to the HONO twisting and the motion of the hydrogen atom involved in ESIPT, respectively. The structural changes associated with PCo1 and PCo2 are illustrated in Fig. 4b. Further explanation of the physical interpretations of PCo1 and PCo2 is provided in Computational Methods section. In **Figure 4a**, the *meta*-IRC pathway is depicted as a red curve from S_0-EQ0 to MECI(S_0/S_1)1. Notably, the ESIPT process is represented

solely along PCo2 from -1.8 to -1.1 amu$^{1/2}$ Å, while the subsequent HONO twisting process is captured along PCo1, spanning from -2.5 to 5.0 amu$^{1/2}$ Å.

Figures 4c-f show the dynamic trajectories projected onto the same two-dimensional subspace. More detailed results are provided in Figs. **change properly**S9-S16. Figure 4c presents 66 trajectories that exhibit ultrafast decay to the S_0 state within 660 fs (= 433 + 227 fs), corresponding to the upper limit of the single-exponential rising signal observed experimentally.[18] These trajectories follow the *meta*-IRC pathway, decaying near MECI(S_0/S_1)1 and forming either *aci*-NP (S_0-EQ3) and *o*-NP (S_0-EQ0, global minimum). In the latter case, most trajectory were terminated shortly after hopping to S_0 due to electronic structure calculation issues. Nevertheless, because S_0-EQ0 is the most stable S_0 structure, these trajectories are assumed to converge there. Similar ultrafast-decay behavior has been reported in the previous *ab initio* multiple spawning (AIMS) simulations,[11] consistent with our findings.

Figure 4d-f illustrate *meta*-IRC-deviating trajectories, most of which undergo ISC to triplet states, with the exception of 12 trajectories shown in Fig. 4d. These 12 trajectories diverge from the *meta*-IRC pathway on the S_1 surface and eventually decay to the *o*-NP region on the S_0 surface. Among them, three trajectories decay after 660 fs. Figures 4e and 4f show 66 trajectories that undergo ISC to the triplet states. Figure 4e displays the portion prior to ISC, while Fig. 4f shows the portion following ISC. These trajectories diverge widely across the S_1 potential energy surface, and all 66 trajectories undergo ISC to triplet states. This result suggests that ISC regions between S_1 and triplet states are delocalized, in contrast to the localized IC region between S_1 and S_0. After hopping to T_1, nearly all trajectories remain trapped in triplet maniforld until 2 ps, with only two trajectories returning to S_0 state via ISC at 1242.75 fs and 1891.75 fs. This observation supports the existence of a long-lived triplet population, as the MESX structures are rarely accessed within the simulation time.

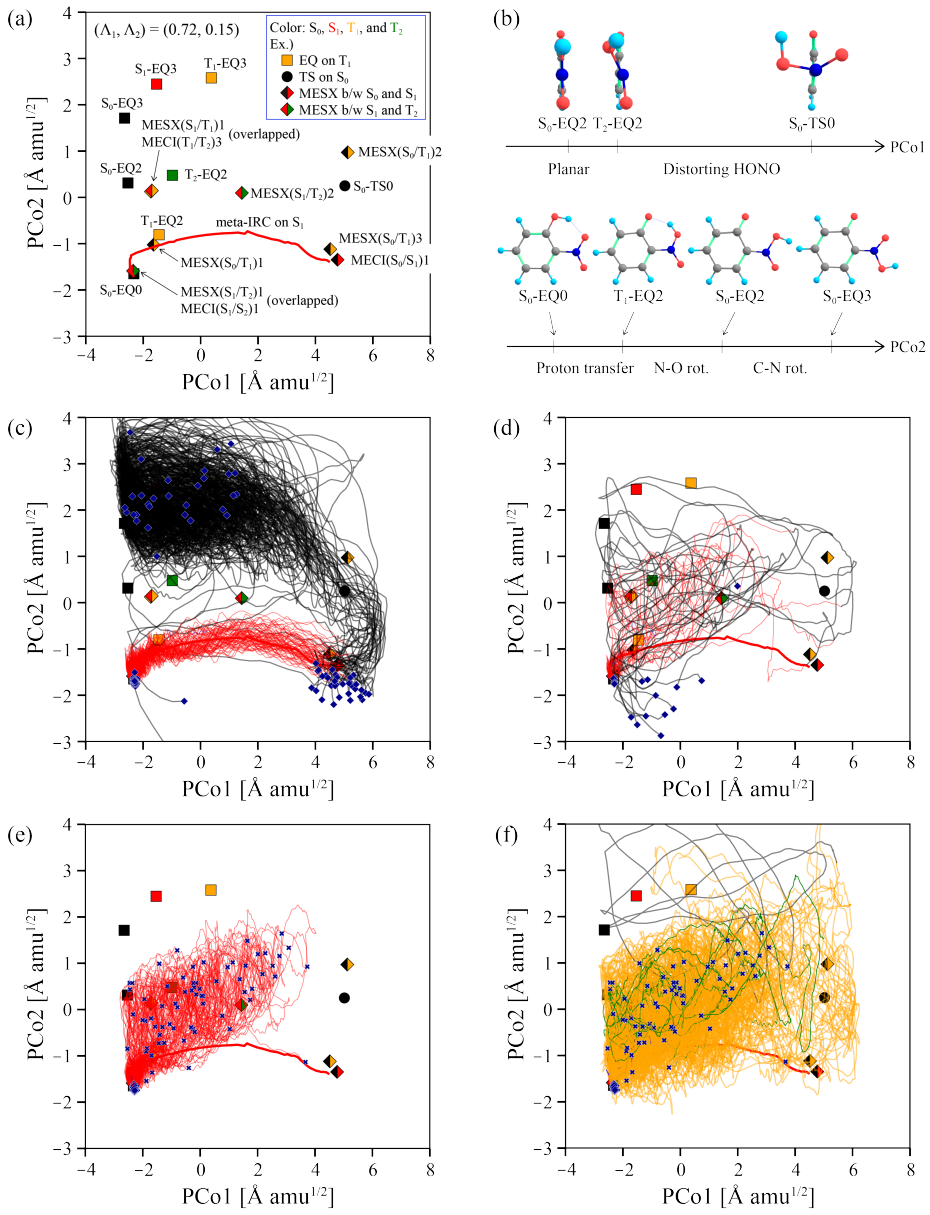

Figure 4: (a) Two-dimensional reaction space determined by ReSPer. The marker colors indicate the electronic states in which the reference structures are involved. EQs and TSs are represented as squares and circles, respectively, while MECIs and MESXs are shown as diamonds in two different colors, corresponding to the electronic states involved in transitions. The *meta*-IRC pathway is also projected as a red line. (b) Molecular structures along the principal coordinates (PCos), PCo1 and PCo2. (c-f) Projected trajectories onto the two-dimensional reaction space from (a): (c) 66 trajectories underwent ultrafast IC to the S_0 state, while (d) 12 trajectories diverged on the S_1 state. For the 66 trajectories that remain in the T_1 state at 2 ps, (e) represents the trajectories in the S_1 state before hopping to the triplet state, and (f) represents the trajectories after hopping to the triplet state.

In conclusion, we have elucidated the origins of the ultrafast-decaying and long-lived signals following $\pi\pi^*$ excitation of *o*-NP using NAMD simulations. In our simulations, upon photoexcitation, *o*-NP undergoes ultrafast ESIPT in the $S_1(\pi\pi^*)$ state with a time constant of 13 fs. Subsequently, a portion of trajectories undergo IC to the S_0 state (339 fs), while the remainder undergoes ISC to triplet states, primarily T_2 (857 fs). The depletion of the S_1 population via these two non-adiabatic processes is believed to correspond to the ultrafast-decaying signals observed in experiments.[15,18] Trajectories hopping to T_2 rapidly relax to T_1 via IC and seldom return to the singlet maniforld, suggesting that *o*-NP in the T_1 state contribute to the long-lived signal. Our simulations propose a new plausible mechanism that accounts for both ultrafast-decaying and long-lived signals observed in photoelectron spectroscopy experiments.[15,18] The time constants obtained for ESIPT and IC are good agreement with previous experimental findings.[15,18] Although time-resolved electron spin resonance (TR-ESR) spectroscopy could serve to validate our assignment, achieving sub-picosecond time resolution remains a challenge. In this study, the combination of NAMD simulations and ReSPer analysis has enabled a comprehensive understanding of the ultrafast dynamics of *o*-NP from a unified perspective of potential energy surfaces and dynamic trajectories. By visualizing dynamic trajectories in the two-dimensional reaction space defined by ReSPer, we identified that the ultrafast decay to the S_0 state is primarily induced by HONO twisting, in agreement with previous reports.[11,15,18] In addition, we newly found that trajectories deviating from the *meta*-IRC on the S_1 surface tend to undergo ISC to triplet states, with the key structural change being the motion of the transferring hydrogen atom. These findings were achieved by the ReSPer analysis without prior knowledge of the mechanisms. Our findings offers new insights into the photoexcited dynamics of *o*-NP and underscores the need for further development of ultrafast time-resolved experimental techniques.

Computational Methods

Energies and gradients for all electronic states were computed using mixed-reference spin-flip time-dependent density functional theory (MRSF-TDDFT)[22,30] as implemented in the GAMESS(US) program package,[31] version 2022 R2. The BH&HLYP functional was employed with the cc-pVDZ basis set.[32] Minimum energy conical intersection (MECI) and minimum energy seam of crossing (MESX) structures were explored using GRRM17,[28,29] interfaced with GAMESS. The GRRM-GAMESS interface, originally developed with an older version of GAMESS in 2011, remains compatible with GAMESS 2022 R2 and MRSF-TDDFT calculations, requiring no additional code modifications. MECI/MESX structures were identified using the artificial force induced reaction (AFIR) method with a gamma parameter of 150 kJ/mol, followed by optimization to actual MECI or MESX structures. On-the-fly surface hopping molecular dynamics simulations were performed using an in-house program[33] with the spin-diabatic scheme. Initial conditions were sampled from a Boltzmann distribution at 300 K. Each trajectory was propagated up to 2 ps using the velocity-Verlet algorithm with a 0.25 fs time step. In our NAMD simulations, the four lowest singlet and three lowest triplet states were included, with SOC constants fixed to 10 cm^{-1} which is the same order of magnitude reported in the previous study.[18] Xu *et al.* [16] reported that fixing SOC constants showed only small differences in dynamics compared to the NAMD simulations with on-the-fly SOC calculations. A total of 144 trajectories were generated; however, some were terminated before 2 ps due to convergence issues in restricted open-shell Kohn-Sham calculations. To improve SCF convergence, each electronic structure calculation was initialized using the previous step's result. If SCF convergence still failed, the trajectory was stopped. Non-adiabatic transitions were accounted for using the Zhu-Nakamura global switching (ZN-GS) algorithm.[23,34] Comparisons between the ZN-GS and Tully's fewest switches (TFS) algorithms have been reported.[33,34] Both methods yield similar results for internal conversion dynamics.[34] For intersystem crossing dynamics, the discrepancy between the two methods strongly depends on the representation of electronic states. Fortunately, when the spin-pure

scheme is employed and the SOC is weak, – as is the case in this study – the ZN-GS and TFS methods produce similar results.[33] Trajectories were analyzed using the ReSPer method,[24–26] which constructs a low-dimensional reaction space that preserves inter-structural distance relationships in the full-dimensional potential energy surfaces. Reference structures selected for the ReSPer analysis included S_0-EQ0, S_0-EQ2, S_0-EQ3, S_1-EQ3, T_1-EQ2, T_1-EQ3, T_2-EQ2, S_0-TS0, MECI(S_0/S_1)1, MECI(S_1/S_2)1, MECI(T_1/T_2)3, MESX(S_0/T_1)1, MESX(S_0/T_1)2, MESX(S_0/T_1)3, MESX(S_1/T_1)1, MESX(S_1/T_2)1, and MESX(S_1/T_2)2, respectively. The *meta*-IRC in the S_1 state and dynamic trajectories were projected using the out-of-sample technique.[25] To interpret the physical meaning of each PCo, we analyzed the molecular structure changes along PCoi while keeping PCoj ($j \neq i$) is constant. The top of Fig. 4b shows the molecular changes along PCo1 with PCo2 $\approx$ 0.5 amu$^{1/2}$ Å, revealing as PCo1 increases, the HONO group (d_{O3N5C6C7}) twists and eventually adopts a pyramidal shape. The bottom of Fig. 4b illustrates the physical meaning of PCo2 with PCo1 $\approx$ -2.5 amu$^{1/2}$ Å, identifying three key transformations: the hydrogen transfer from -1.8 to -1.1 amu$^{1/2}$ Å, the formation of non-hydrogen bonding (*aci*-NP) structures, related to rotation of d_{C6N5O3H2} from -0.8 to 0.5 amu$^{1/2}$ Å, and the rotation of the HONO group involving changes in d_{O3N5C6C7} from 0.5 to 1.8 amu$^{1/2}$ Å.

Conflicts of interest

The authors declare no competing financial interest.

Acknowledgement

This work was partly supported by the Photo-excitonix Project in Hokkaido University, JST CREST Grant Number JPMJCR1902, MEXT Program of Data Creation and Utilization-Type Material Research and Development Project Grant Number JPMXP1122712807, JST ACT-X Grant Number JPMJAX23DE, and JSPS KAKENHI Grant Number JP22K14649.

A part of the calculations was performed using the Research Center for Computational Science, Okazaki, Japan (Project: 23-IMS-C016).

Supporting Information Available

Calculated absorption spectra of *o*-NP at the MRSF-TDDFT level; Comparison between CASPT2 and MRSF-TDDFT results; The number of surviving trajectories over the course of the simulations; Histograms of hopping times between electronic states; Fitting functions based on first-order kinetics for electronic population; Time evolution of the absolute value of the dihedral angle; Minimum energy conical intersection (MECI) / minimum energy seam of crossing (MESX) structures; Dynamically accessed MECI/MESX structures with the number of transitions near each structure; Trajectory classification by reaction space projector (ReSPer) analysis

References

(1) Laskin, A.; Laskin, J.; Nizkorodov, S. A. Chemistry of Atmospheric Brown Carbon. *Chemical Reviews* **2015**, *115*, 4335–4382.

(2) Hinrichs, R. Z.; Buczek, P.; Trivedi, J. J. Solar absorption by aerosol-bound nitrophenols compared to aqueous and gaseous nitrophenols. *Environmental Science & Technology* **2016**, *50*, 5661–5667.

(3) Sangwan, M.; Zhu, L. Absorption cross sections of 2-nitrophenol in the 295–400 nm region and photolysis of 2-nitrophenol at 308 and 351 nm. *The Journal of Physical Chemistry A* **2016**, *120*, 9958–9967.

(4) Sangwan, M.; Zhu, L. Role of methyl-2-nitrophenol photolysis as a potential source of OH radicals in the polluted atmosphere: implications from laboratory investigation. *The Journal of Physical Chemistry A* **2018**, *122*, 1861–1872.

(5) Gligorovski, S.; Strekowski, R.; Barbati, S.; Vione, D. Environmental implications of hydroxyl radicals (• OH). *Chemical reviews* **2015**, *115*, 13051–13092.

(6) An, M.; Kim, B.-Y.; Seo, H.; Helal, A.; Kim, H.-S. Fluorescence sensor for sequential detection of zinc and phosphate ions. *Spectrochimica Acta Part A: Molecular and Biomolecular Spectroscopy* **2016**, *169*, 87–94.

(7) Sedgwick, A. C.; Wu, L.; Han, H.-H.; Bull, S. D.; He, X.-P.; James, T. D.; Sessler, J. L.; Tang, B. Z.; Tian, H.; Yoon, J. Excited-state intramolecular proton-transfer (ESIPT) based fluorescence sensors and imaging agents. *Chemical Society Reviews* **2018**, *47*, 8842–8880.

(8) Mamada, M.; Inada, K.; Komino, T.; Potscavage Jr, W. J.; Nakanotani, H.; Adachi, C. Highly efficient thermally activated delayed fluorescence from an excited-state intramolecular proton transfer system. *ACS central science* **2017**, *3*, 769–777.

(9) Wu, K.; Zhang, T.; Wang, Z.; Wang, L.; Zhan, L.; Gong, S.; Zhong, C.; Lu, Z.-H.; Zhang, S.; Yang, C. De novo design of excited-state intramolecular proton transfer emitters via a thermally activated delayed fluorescence channel. *Journal of the American Chemical Society* **2018**, *140*, 8877–8886.

(10) Bailey-Darland, S.; Krueger, T. D.; Fang, C. Ultrafast spectroscopies of nitrophenols and nitrophenolates in solution: From electronic dynamics and vibrational structures to photochemical and environmental implications. *Molecules* **2023**, *28*, 601.

(11) Nunes, J. P. F. et al. Photo-induced structural dynamics of o-nitrophenol by ultrafast electron diffraction. *Physical Chemistry Chemical Physics* **2024**, *26*, 17991–17998.

(12) Vandaele, E.; Mališ, M.; Luber, S. The Role of Aqueous Solvation on the Intersystem Crossing of Nitrophenols. *Journal of Chemical Theory and Computation* **2024**, *20*, 3258–3272.

(13) Greene, H. J. M.; Ghosh, D.; Sazanovich, I. V.; Phelps, R.; Curchod, B. F. E.; Orr-Ewing, A. J. Competing Nonadiabatic Relaxation Pathways for Near-UV Excited *ortho*-Nitrophenol in Aqueous Solution. *The Journal of Physical Chemistry Letters* **2024**, *15*, 9153–9159.

(14) Yin, B.-W.; Wang, J.-L.; Dai, J.-l.; Jian, J.-W.; Jia, P.-K.; Cui, G.; Xie, B.-B. Excited-State Decay and Photolysis of *O*-Nitrophenol after Proton Transfer. II: A Theoretical Investigation in the Microsolvated Atmospheric Environment. *The Journal of Physical Chemistry A* **2024**, *128*, 9486–9496.

(15) Ernst, H. A.; Wolf, T. J.; Schalk, O.; González-García, N.; Boguslavskiy, A. E.; Stolow, A.; Olzmann, M.; Unterreiner, A.-N. Ultrafast dynamics of *o*-nitrophenol: An experimental and theoretical study. *The Journal of Physical Chemistry A* **2015**, *119*, 9225–9235.

(16) Xu, C.; Yu, L.; Zhu, C.; Yu, J.; Cao, Z. Intersystem crossing-branched excited-state intramolecular proton transfer for *o*-nitrophenol: An ab initio on-the-fly nonadiabatic molecular dynamic simulation. *Scientific Reports* **2016**, *6*, 26768.

(17) Ciavardini, A.; Coreno, M.; Callegari, C.; Spezzani, C.; De Ninno, G.; Ressel, B.; Grazioli, C.; de Simone, M.; Kivimaki, A.; Miotti, P.; others Ultra-fast-VUV photoemission study of UV excited 2-nitrophenol. *The Journal of Physical Chemistry A* **2019**, *123*, 1295–1302.

(18) Nitta, Y.; Schalk, O.; Igarashi, H.; Wada, S.; Tsutsumi, T.; Saita, K.; Taketsugu, T.; Sekikawa, T. Real-time probing of an atmospheric photochemical reaction by ultrashort extreme ultraviolet pulses: Nitrous acid release from o-nitrophenol. *The Journal of Physical Chemistry Letters* **2021**, *12*, 674–679.

(19) Guthmuller, J. Assessment of TD-DFT and CC2 methods for the calculation of res-

onance Raman intensities: application to *o*-nitrophenol. *Journal of Chemical Theory and Computation* **2011**, *7*, 1082–1089.

(20) Takezaki, M.; Hirota, N.; Terazima, M. Nonradiative relaxation processes and electronically excited states of nitrobenzene studied by picosecond time-resolved transient grating method. *The Journal of Physical Chemistry A* **1997**, *101*, 3443–3448.

(21) El-Sayed, M. A. Spin—Orbit Coupling and the Radiationless Processes in Nitrogen Heterocyclics. *The Journal of Chemical Physics* **1963**, *38*, 2834–2838.

(22) Lee, S.; Filatov, M.; Lee, S.; Choi, C. H. Eliminating spin-contamination of spin-flip time dependent density functional theory within linear response formalism by the use of zeroth-order mixed-reference (MR) reduced density matrix. *The Journal of Chemical Physics* **2018**, *149*, 104101.

(23) Yu, L.; Xu, C.; Lei, Y.; Zhu, C.; Wen, Z. Trajectory-based nonadiabatic molecular dynamics without calculating nonadiabatic coupling in the avoided crossing case: trans $\leftrightarrow$ cis photoisomerization in azobenzene. *Physical Chemistry Chemical Physics* **2014**, *16*, 25883–25895.

(24) Tsutsumi, T.; Ono, Y.; Arai, Z.; Taketsugu, T. Visualization of the intrinsic reaction coordinate and global reaction route map by classical multidimensional scaling. *Journal of Chemical Theory and Computation* **2018**, *14*, 4263–4270.

(25) Tsutsumi, T.; Ono, Y.; Arai, Z.; Taketsugu, T. Visualization of the dynamics effect: projection of on-the-fly trajectories to the subspace spanned by the static reaction path network. *Journal of Chemical Theory and Computation* **2020**, *16*, 4029–4037.

(26) Tsutsumi, T.; Ono, Y.; Taketsugu, T. Visualization of reaction route map and dynamical trajectory in reduced dimension. *Chemical Communications* **2021**, *57*, 11734–11750.

(27) Tachibana, A.; Fukui, K. Differential geometry of chemically reacting systems. *Theoretica chimica acta* **1978**, *49*, 321–347.

(28) Maeda, S.; Ohno, K.; Morokuma, K. Systematic exploration of the mechanism of chemical reactions: the global reaction route mapping (GRRM) strategy using the ADDF and AFIR methods. *Physical Chemistry Chemical Physics* **2013**, *15*, 3683.

(29) Maeda, S.; Harabuchi, Y.; Sumiya, Y.; Takagi, M.; Suzuki, K.; Hatanaka, M.; Osada, Y.; Taketsugu, T.; Morokuma, K.; Ohno, K. GRRM17. `http://iqce.jp/GRRM/index_e.shtml`, Accessed: 2025-04-16.

(30) Lee, S.; Kim, E. E.; Nakata, H.; Lee, S.; Choi, C. H. Efficient implementations of analytic energy gradient for mixed-reference spin-flip time-dependent density functional theory (MRSF-TDDFT). *The Journal of Chemical Physics* **2019**, *150*, 184111.

(31) Barca, G. M. J. et al. Recent developments in the general atomic and molecular electronic structure system. *The Journal of Chemical Physics* **2020**, *152*, 154102.

(32) Dunning, T. H. Gaussian basis sets for use in correlated molecular calculations. I. The atoms boron through neon and hydrogen. *The Journal of Chemical Physics* **1989**, *90*, 1007–1023.

(33) Wada, S.; Tsutsumi, T.; Saita, K.; Taketsugu, T. Ab initio molecular dynamics study of intersystem crossing dynamics for MH_2 (M= Si, Ge, Sn, Pb) on spin-pure and spin-mixed potential energy surfaces. *Journal of Computational Chemistry* **2024**, *45*, 552–562.

(34) Yue, L.; Yu, L.; Xu, C.; Lei, Y.; Liu, Y.; Zhu, C. Benchmark performance of global switching versus local switching for trajectory surface hopping molecular dynamics simulation: cis $\leftrightarrow$ trans azobenzene photoisomerization. *ChemPhysChem* **2017**, *18*, 1274–1287.

TOC Graphic

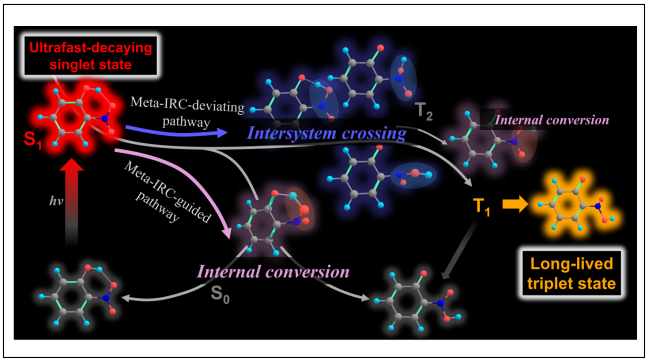
Ultrafast-decaying singlet state
S1
Meta-IRC-deviating pathway
Intersystem crossing
T2
Internal conversion
T1
Long-lived triplet state
hν
Meta-IRC-guided pathway
Internal conversion
S0